

## FIRST DETECTION OF AMMONIA IN M 82

A. WEISS

Radioastronomisches Institut der Universität Bonn, Auf dem Hügel 71, 53121 Bonn, Germany  
aweiss@astro.uni-bonn.de

N. NEININGER

Radioastronomisches Institut der Universität Bonn, Auf dem Hügel 71, 53121 Bonn, Germany

C. HENKEL

Max-Planck-Institut für Radioastronomie, Auf dem Hügel 69, 53121 Bonn, Germany

J. STUTZKI

I. Physikalisches Institut der Universität zu Köln, Zülpicher Straße 77, 50937 Köln, Germany

AND

U. KLEIN

Radioastronomisches Institut der Universität Bonn, Auf dem Hügel 71, 53121 Bonn, Germany

## ABSTRACT

We report the detection of the (J,K) = (1,1), (2,2), and (3,3) inversion lines of ammonia (NH<sub>3</sub>) towards the south-western molecular lobe in M 82. The relative intensities of the ammonia lines are characterized by a rotational temperature of  $T_{rot} = 29 \pm 5$  K which implies an average kinetic temperature of  $T_{kin} \approx 60$  K. A Gaussian decomposition of the observed spectra indicates increasing kinetic temperatures towards the nucleus of M 82, consistent with recent findings based on CO observations. The observations imply a very low NH<sub>3</sub> abundance relative to H<sub>2</sub>,  $X(\text{NH}_3) \approx 5 \times 10^{-10}$ . We present evidence for a decreasing NH<sub>3</sub> abundance towards the central active regions in M 82 and interpret this abundance gradient in terms of photodissociation of NH<sub>3</sub> in PDRs. The low temperature derived here from NH<sub>3</sub> also explains the apparent underabundance of complex molecules like CH<sub>3</sub>OH and HNCO, which has previously been reported.

*Subject headings:* galaxies:individual (M 82)–galaxies:ISM–galaxies:starburst–ISM:abundance–radio lines:ISM

## 1. INTRODUCTION

The physical properties of molecular clouds are important parameters which are believed to influence largely the rate at which stars can form by gravitational collapse of cloud fragments. The nearby starburst galaxy M 82 is known to host a large amount of molecular gas ( $M(\text{H}_2) \approx 1 \times 10^8 \text{M}_\odot$ , e.g. Wild et al. (1992)) and is currently undergoing a phase of intense star formation. Therefore it has been a prime target to determine the physical conditions of the molecular phase of its ISM in order to increase our understanding of the relevant physical processes connected with violent star formation activity.

Most of these studies use CO emission lines to derive the physical properties of the molecular gas (e.g. Harris et al. (1991); Wild et al. (1992), and more recently Mao et al. (2000); Petitpas & Wilson (2000); Weiß et al. (2001)). Yet the interpretation of CO emission lines requires the application of radiative transfer models which use simplifying assumptions about the structure and kinematics of molecular clouds. Therefore it is desirable to observe other molecules which directly trace the physical conditions and thus allow a test of conclusions gained from CO observations. Ammonia (NH<sub>3</sub>) is such a molecule: the relative population of its meta-stable inversion lines is sensitive to the kinetic gas temperature (e.g. Walmsley & Ungerechts (1983)). Therefore observations of ammonia inversion lines can be used as a molecular cloud thermometer. Here we report the first detection of ammonia towards the most

prominent molecular source in M 82, the south-western molecular lobe. We compare our interpretation of the ammonia lines to conclusions deduced from CO observations.

## 2. OBSERVATIONS

The (J,K) = (1,1), (2,2), (3,3) and (4,4) inversion lines of ammonia were observed towards the south-western (SW) molecular lobe in M 82 ( $\alpha_{2000} = 09^h 55^m 49.06^s$ ,  $\delta_{2000} = 69^\circ 40' 41''.2$ ) using the Effelsberg 100 m telescope of the MPIfR equipped with a dual channel K-band HEMT receiver. The system temperature was 180–200 K on a main beam brightness temperature ( $T_{mb}$ ) scale. The observations were carried out in May 2000 and Feb. 2001. The beam size of the 100-m telescope at 23 GHz is  $\approx 40''$ . The data were recorded using an autocorrelator with  $8 \times 512$  channels and a bandwidth of 40 MHz for each backend, leading to a channel spacing of  $1 \text{ km s}^{-1}$ . The eight backends were configured such that all four ammonia lines were observed simultaneously. Each pair of backends centered on a given ammonia line was used to sample both linear polarizations independently. To avoid a contamination of the data by low-level baseline instabilities we shifted the center velocity of the backends (May 2000) and permuted the backends (Feb. 2001) every 90 minutes. The measurements were carried out in dual-beam switching mode, with a switching frequency of 1 Hz and a beam throw of 2' in azimuth. Flux calibration was obtained by observing both the continuum and the ammonia lines of

W3(OH) before each observing run (for fluxes see Mauersberger, Wilson, & Henkel (1988) and Ott et al. (1994)). Pointing was checked every 1.5 hours on the nearby continuum source 0836+71 and was found to be stable to within  $5 - 10''$ . A linear baseline was removed from each spectrum and intensities were converted to a  $T_{mb}$  scale. The summed spectra were smoothed to a velocity resolution of  $16 \text{ km s}^{-1}$ . We estimate the flux calibration of the final reduced spectra to be accurate within  $\pm 20\%$  (10% error of the flux calibration and 10% uncertainty due to low-level baseline instabilities).

### 3. RESULTS

The observed spectra of the ammonia lines are shown in Fig. 1. The  $(J,K) = (1,1) - (3,3)$  lines are detected with a S/N ratio better than 4. The  $(4,4)$  line is not detected. The  $(1,1)$  and  $(2,2)$  lines peak at  $v_{lsr} = 100 \text{ km s}^{-1}$  ( $C_{100}$ ) and show a weaker component at  $v_{lsr} = 160 \text{ km s}^{-1}$  ( $C_{160}$ ). Both velocity components are also detected in low- and mid-J CO emission lines (see e.g. Harris et al. (1991); Wild et al. (1992); Mao et al. (2000); Petitpas & Wilson (2000)). At  $40''$  resolution the intensity of the low-J CO transitions from  $C_{160}$  is stronger than that from  $C_{100}$ . To emphasize this point we show the line profile of the  $^{12}\text{CO}(J = 1 \rightarrow 0)$  transition at  $40''$  resolution in the top panel of Fig. 1.

Beam averaged column densities for individual inversion states were calculated using

$$N(J, K) = \frac{7.77 \cdot 10^{13}}{\nu} \frac{J(J+1)}{K^2} \int T_{mb} dv \quad (1)$$

(e.g. Henkel et al. (2000)). The column density  $N$ , the frequency  $\nu$  and the integrated line intensity are in units of  $\text{cm}^{-2}$ , GHz and  $\text{K km s}^{-1}$ , respectively. Line parameters and column densities are summarized in Tab. 1. Note that this approximation assumes optically thin emission and the contribution of the  $2.7 \text{ K}$  background to be negligible ( $T_{ex} \gg 2.7 \text{ K}$ ). Following the analysis described by Henkel et al. ((2000)) the rotation temperature ( $T_{rot}$ ) between levels  $J$  and  $J'$  can be determined from the slope of a linear fit in the rotation diagram (normalized column density vs. energy above the ground state expressed in  $E/k$ ) by

$$T_{rot} = \frac{-\log(e)}{a} = \frac{-0.434}{a} \quad (2)$$

where  $a$  is the slope of the linear fit.

The rotation diagram for the observed ammonia lines is shown in Fig. 2. The rotation temperature between the  $(1,1)$  and  $(2,2)$  inversion levels of para-ammonia is  $T_{rot} = 29 \text{ K}$  (thick solid line). The uncertainty, derived from the extrema of the slope including the  $(4,4)$  level as an upper limit, is  $\pm 5 \text{ K}$  (dotted lines). The  $(J,K) = (3,3)$  line is not included in the fit because it belongs to ortho-ammonia, thus to a different ammonia species. Nevertheless, it nicely fits to the rotation temperature derived from the two lowest inversion levels of para-ammonia.

In addition to the analysis of the integrated line intensities we have decomposed the  $(J,K) = (1,1)$  and  $(2,2)$  spectra into two Gaussian components with fixed center velocities of  $v_{lsr} = 100 \text{ km s}^{-1}$  ( $C_{100}$ ) and  $160 \text{ km s}^{-1}$  ( $C_{160}$ ). The Gaussian decomposition is shown together with the

observed line profile in the two top panels of Fig. 1. A separate analysis of the rotation temperatures between the  $(1,1)$  and  $(2,2)$  inversion levels for both components yields  $T_{rot,100} = 24_{-6}^{+12} \text{ K}$  and  $T_{rot,160} = 31_{-10}^{+22} \text{ K}$  for  $C_{100}$  and  $C_{160}$ , respectively. For the errors we have assumed 30% uncertainty from the Gaussian decomposition. Note that the observed upper limit for the  $(J,K) = (4,4)$  line intensity is still consistent with the shallow slope derived for the emission arising from the  $160 \text{ km s}^{-1}$  component ( $C_{160}$ ).

## 4. DISCUSSION

### 4.1. The $\text{NH}_3$ emitting volume

High-spatial resolution CO observations show that the emission at  $v_{lsr} \approx 100 \text{ km s}^{-1}$  is mainly associated with the SW molecular lobe. The emission at  $v_{lsr} \approx 160 \text{ km s}^{-1}$  arises from regions closer to the nucleus, i.e. from the central molecular peak and the inner CO outflow region. Thus  $C_{160}$  covers the regions of the western mid infrared peak close to the central molecular peak (Telesco & Gezari (1992)), and the region where an expanding molecular superbubble was identified (Weiβ et al. (1999)). Therefore  $C_{160}$  represents a more active region than the outer molecular lobe itself. An overlay of the two regions at high spatial resolution ( $\approx 2''$ ) as observed in the  $^{12}\text{CO}(J = 2 \rightarrow 1)$  transition (Weiβ et al. (2001)) is shown in Fig. 3.

### 4.2. Comparison with temperature determinations from other line observations

Radiative transfer calculations (e.g. Walmsley & Ungerichts (1983)) of  $\text{NH}_3$  show that rotation temperatures determined from meta-stable levels only reflect the kinetic gas temperature for low ( $T < 15 \text{ K}$ ) temperatures. For larger temperatures the rotation temperature largely underestimates the kinetic gas temperature due to depopulation mechanisms. Correcting our results for these effects, our mean rotation temperature of  $29 \text{ K}$  corresponds to a mean kinetic temperature of  $T_{kin} \approx 60 \text{ K}$ . Using the Gaussian decomposition we find  $T_{kin} \approx 45 \text{ K}$  for the temperature in the SW molecular lobe ( $C_{100}$ ), and  $T_{kin} \approx 80 \text{ K}$  for the regions closer to the nucleus ( $C_{160}$ ).

These values are in good agreement with recent high-resolution kinetic temperature estimates using radiative transfer calculations based on CO observations by Weiβ et al. ((2001)). They derive  $T_{kin} \approx 55 \text{ K}$  for the SW molecular lobe, and an average of  $T_{kin} \approx 110 \text{ K}$  over the region which corresponds to  $C_{160}$  in our study. The simultaneous observations of two [C I] fine structure lines towards the SW lobe allowed Stutzki et al. ((1997)) to derive a lower limit for the kinetic temperature of the [C I] emitting gas in  $C_{100}$  of  $50 \text{ K}$  which is consistent with the temperature derived above from the  $\text{NH}_3$  lines. Similar values ( $T_{kin} = 50 \text{ K}$ ) have been found by Seaquist & Frayer ((2000)) using  $\text{HCO}^+$  and  $\text{HCN}$  emission lines.

Note, however, that the uncertainty of the kinetic temperature estimates from the Gaussian decomposition of the  $\text{NH}_3$  spectra is quite large. Nevertheless, the results are in line with the general picture that the kinetic temperature rises from the outer parts of the SW molecular lobe towards the active regions closer to the nucleus of M 82. In comparison with rotation temperatures determined from  $\text{NH}_3$  in IC 342 ( $T_{rot} \approx 50 \text{ K}$ ; Martin & Ho (1986)) and Maffei 2 ( $T_{rot} \approx 85 \text{ K}$ ; Henkel et al. (2000)) the values

determined here for M 82 are very low. Thus the temperature of the dense molecular gas in M 82 is obviously much lower than in other galaxies with large nuclear concentrations of molecular gas. This explains the apparent underabundance of molecules like SiO, CH<sub>3</sub>OH, HNCO, and CH<sub>3</sub>CN in M 82 which only form in a dense and *warmer* environment (see e.g. Mauersberger & Henkel (1993)).

#### 4.3. NH<sub>3</sub> abundance

Using eq. A15 of Ungerechts, Walmsley, & Winnewisser ((1986)) we have estimated a total beam-averaged NH<sub>3</sub> column density of  $N(\text{NH}_3) \approx 1 \times 10^{13} \text{ cm}^{-2}$ . The beam-averaged H<sub>2</sub> column density was estimated to be  $N(\text{H}_2) \approx 1.9 \times 10^{22} \text{ cm}^{-2}$  using the CO spectrum shown in Fig. 1 and a conversion factor of  $X_{\text{CO}} = 5 \times 10^{19} \text{ cm}^{-2} (\text{K km s}^{-1})^{-1}$ , which corresponds to the average value of the conversion factors derived by Weiß et al. ((2001)) in the region covered by 100–180 km s<sup>-1</sup> emission. This yields a relative abundance of ammonia of  $X(\text{NH}_3) \approx 5 \times 10^{-10}$ , which is an extremely low value. In nearby dark clouds the fractional NH<sub>3</sub> abundance is of order  $X(\text{NH}_3) \approx 10^{-7}$  (e.g. Benson & Myers (1983)) and in hot cores NH<sub>3</sub> is even more abundant ( $X(\text{NH}_3) \approx 10^{-5} \dots -6$ ; e.g. Mauersberger, Henkel & Wilson (1987)). In a recent work on Maffei 2 Henkel et al. ((2000)) found  $X(\text{NH}_3) \approx 10^{-8}$ .

A closer look at the (J,K)=(1,1) and the <sup>12</sup>CO( $J = 1 \rightarrow 0$ ) spectra displayed in Fig. 1 (top) reveals another interesting aspect regarding the spatial variation of the NH<sub>3</sub> abundance: the line temperature ratio  $T(\text{NH}_3(1,1))/T(^{12}\text{CO}(J=1 \rightarrow 0))$  decreases with increasing velocity for  $v_{lsr} > 100 \text{ km s}^{-1}$ . The solid-body rotation in the inner part of M 82 allows one to associate velocities lower than the systemic velocity of  $v_{lsr} = 230 \text{ km s}^{-1}$  with a specific distance from the nucleus (e.g. Neininger et al. (1998)). Therefore,  $T(\text{NH}_3(1,1))$  per velocity interval traces the ammonia column density in a

region much smaller than the spatial resolution, while  $T(^{12}\text{CO}(J=1 \rightarrow 0))$  traces the H<sub>2</sub> column density. Note that conversion from I(CO) to  $N(\text{H}_2)$  changes across the major axis of M 82 and therefore for each velocity interval (Weiß et al. (2001)). Fig. 4 shows a histogram with  $X(\text{NH}_3)$  versus radial velocity and galactocentric radius, accounting for variations of  $X_{\text{CO}}$  as determined by Weiß et al. ((2001)). The NH<sub>3</sub> abundance is found to decrease towards the center of M 82. We believe that this finding reflects a real change of the ammonia abundance, because a constant NH<sub>3</sub> abundance would imply that  $X_{\text{CO}}$  changes by a factor of more than 40 on a linear scale of 300 pc which is not consistent with radiative transfer models. Due to its low energy threshold for photodissociation ( $\approx 4.1 \text{ eV}$ , Suto & Lee (1983)), NH<sub>3</sub> should be destroyed rapidly in PDRs (Güsten & Fiebig (1988)). This process should be even more efficient when the bulk of the gas is distributed in a diffuse phase with low H<sub>2</sub> column densities as it seems to be true for the central regions in M 82 (Mao et al. (2000), Weiß et al. (2001)). In such an environment shielding against the strong UV radiation is ineffective which leads to low NH<sub>3</sub> abundances towards the central star forming regions. Note, that NH<sub>3</sub> abundances are not always small in a warm environment. Efficient release of NH<sub>3</sub> into the gas phase by evaporation of dust grain mantles is known to occur in galactic ‘hot cores’. This process, however, becomes efficient at slightly higher temperatures than those obtained by us for NH<sub>3</sub> in Sect. 4.2. We therefore interpret the abundance gradient as a result of ammonia being almost completely dissociated in the harsh environment close to M 82’s nucleus, whereas it can still partially survive, with low abundance, in the cooler, denser, and thus better shielded, clouds of the SW lobe.

This research project was supported by the Deutsche Forschungsgemeinschaft grant SFB 494.

#### REFERENCES

Benson, P.J., & Myers, P.C., 1983, ApJ, 270, 589  
 Güsten, R., & Fiebig, D., 1988, A&A, 204, 253  
 Harris, A.I., Hills, R.E., Stutzki, J., Graf, U.U., Russell, A.P.G., & Genzel, R., 1991, ApJ 382, L75  
 Henkel, C., Mauersberger, R., Peck, A.B., Falcke, H., & Hagiwara, Y., 2000, A&A, 361, L45  
 Mao, R.Q., Henkel, C., Schulz, A., Zielsky, M., Mauersberger, R., Störzer, H., Wilson, T.L., & Gensheimer, P., 2000, A&A, 358, 433  
 Martin, R.N., & Ho, P.T.P., 1986, ApJ, 308, L7  
 Mauersberger, R., & Henkel, C., 1993, Reviews of Modern Astronomy Vol.6, 69  
 Mauersberger, R., Henkel, C., & Wilson, T.L., 1987, A&A, 173, 352  
 Mauersberger, R., Wilson, T.L., & Henkel, C., 1988, A&A, 201, 123  
 Neininger, N., Guèlin, M., Klein, U., García-Burillo, S., & Wielebinski, R., 1998, A&A, 339, 737  
 Ott, M., Witzel, A., Quirrenbach, A., Krichbaum, T.P., Standke, K.J., Schalinski, C.J., & Hummel, C.A., 1994, A&A, 284, 331  
 Petitpas, G.R., & Wilson, C.D., 2000, ApJ, 538, 117  
 Seaquist, E.R., & Frayer, D.T., 2000, ApJ, 540, 765  
 Stutzki, J., Graf, U.U., Haas, S., et al. 1997, ApJ 477, L33  
 Suto, M., & Lee, L.C., 1983, J. Chem. Phys., 78, 4515  
 Telesco, C.M., & Gezari, D.Y., 1992, ApJ, 395, 461  
 Walmsley, C.M., & Ungerechts, H., 1983, A&A, 122, 164  
 Weiß, A., Neininger, N., Hüttemeister, S., & Klein, U., 2001, A&A, 365, 571  
 Weiß, A., Walter, F., Neininger, N., & Klein, U., 1999, A&A, 345, L23  
 Wild, W., Harris, A.I., Eckart, A., Genzel, R., Graf, U.U., Jackson, J.M., Russell, A.P.G., & Stutzki, J., 1992, A&A, 265, 447  
 Ungerechts, H., Walmsley, C.M., & Winnewisser, G., 1986, A&A, 157, 207

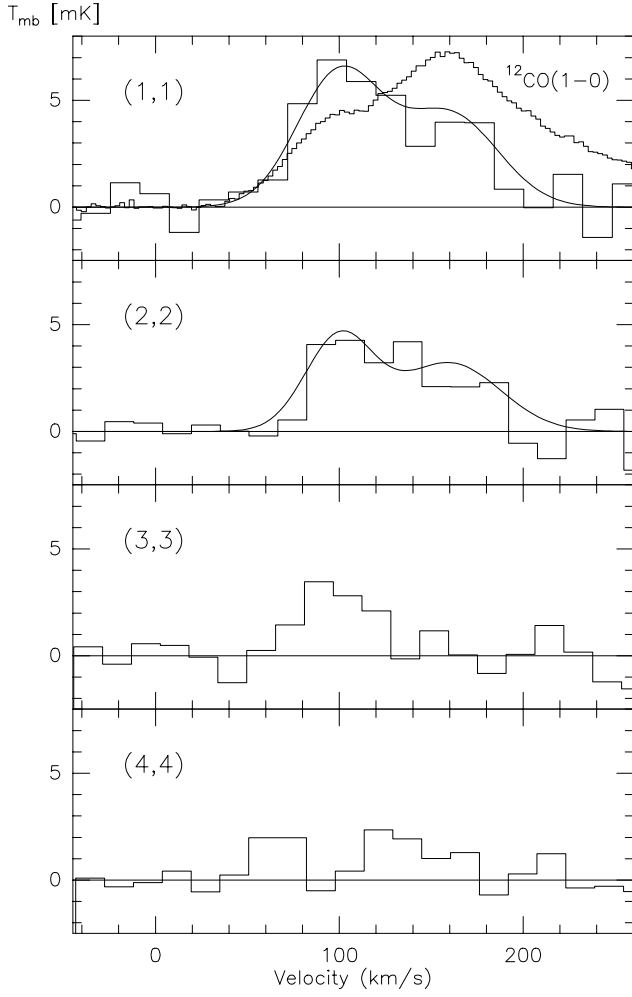


FIG. 1.— NH<sub>3</sub> spectra towards the SW part of M 82 ( $\alpha_{2000} = 09^h 55^m 49.06^s$ ,  $\delta_{2000} = 69^\circ 40' 41''$ .2). The velocity resolution is  $16 \text{ km s}^{-1}$  for each spectrum. The high-resolution spectrum in the top panel shows the  $^{12}\text{CO}(J=1 \rightarrow 0)$  emission line at the same position and spatial resolution ( $40''$ ) scaled by 1/370. For the fits to the (1,1) and (2,2) lines see Sect. 3.

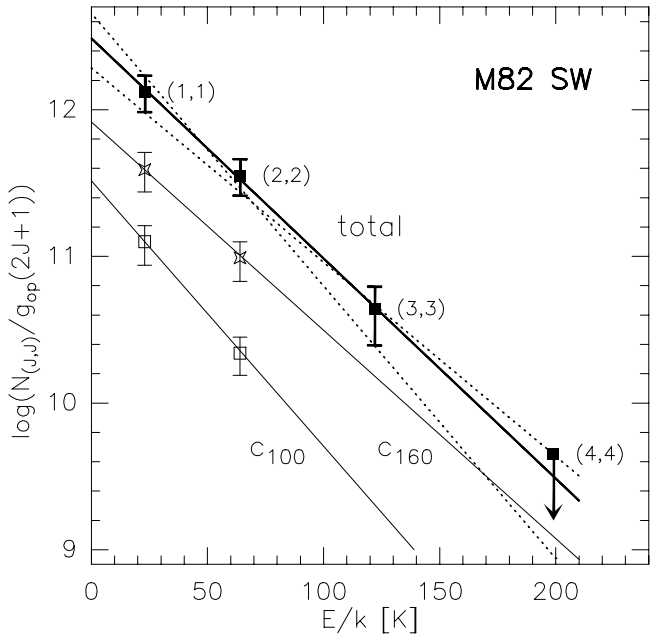


FIG. 2.— Rotation diagram of meta-stable ammonia transitions towards the SW molecular lobe in M82. The filled squares show the normalized column densities determined from the integrated line intensities. The thick solid line (denoted by 'total') corresponds to a linear fit to the  $(J,K) = (1,1)$  and  $(2,2)$  lines for these values. The dotted lines correspond to the linear fits with the lowest and highest slope, which are still consistent with the data including the upper limit for the  $(J,K) = (4,4)$  line. The open squares and the stars show the normalized column densities determined from a Gaussian decomposition of the  $(J,K) = (1,1)$  and  $(2,2)$  spectra into the velocity components  $C_{100}$  and  $C_{160}$ . Note that for display purpose the values for  $C_{160}$  and  $C_{100}$  have been shifted by  $-0.2$  and  $-0.8$  on the y-axis scale, respectively. The thin solid lines correspond to linear fits to these data points.

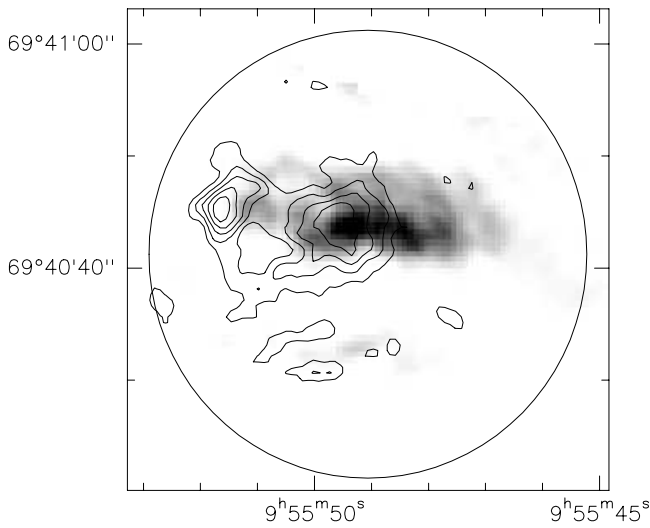


FIG. 3.— High-spatial resolution  $^{12}\text{CO}(J=2 \rightarrow 1)$  data integrated over  $v_{lsr} = 130 - 190 \text{ km s}^{-1}$  ( $C_{160}$ , contours) juxtaposed on  $^{12}\text{CO}(J=2 \rightarrow 1)$  data integrated over  $v_{lsr} = 80 - 120 \text{ km s}^{-1}$  ( $C_{100}$ , greyscale). The  $40''$  beam size of the Effelsberg telescope is indicated by the circle.

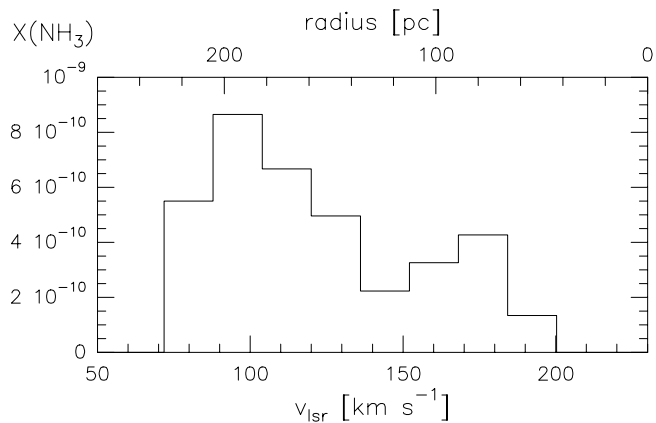


FIG. 4.— NH<sub>3</sub> abundance relative to H<sub>2</sub> per velocity interval. The upper axis denotes the distance of the emission region from the nucleus of M 82 assuming pure solid body rotation and a velocity gradient of 0.7 km s<sup>-1</sup> pc<sup>-1</sup>.

TABLE 1

PARAMETERS OF THE AMMONIA LINES TOWARDS THE SW MOLECULAR LOBE OF M 82. COLUMN 2 TO 6 CORRESPOND TO THE LINE PARAMETERS OF THE ENTIRE LINE PROFILES DERIVED FROM A VISUAL INSPECTION. COLUMNS 7 AND 8 GIVE THE COLUMN DENSITIES FOR THE (1,1) AND (2,2) TRANSITIONS DERIVED FROM A GAUSSIAN DECOMPOSITION OF THE SPECTRA.

Transition (J,K)	$T_{mb}^{peak}$ (mK)	$\int T_{mb} dv$ (K km s $^{-1}$ )	$V_{LSR}^{peak}$ (km s $^{-1}$ )	$\Delta V_{1/2}$ (km s $^{-1}$ )	$N(J, K)$ (10 $^{12}$ cm $^{-2}$ )	$N(J, K)_{100}$ (10 $^{12}$ cm $^{-2}$ )	$N(J, K)_{160}$ (10 $^{12}$ cm $^{-2}$ )
(1,1)	$6.9 \pm 0.8$	$0.61 \pm 0.16$	$97 \pm 16$	$94 \pm 11$	$4.0 \pm 1.1$	$2.2 \pm 0.8$	$1.8 \pm 0.6$
(2,2)	$4.3 \pm 0.9$	$0.36 \pm 0.11$	$105 \pm 16$	$80 \pm 10$	$1.8 \pm 0.5$	$0.9 \pm 0.3$	$1.0 \pm 0.3$
(3,3)	$3.5 \pm 0.7$	$0.14 \pm 0.06$	$95 \pm 10$	$47 \pm 20$	$0.6 \pm 0.26$	—	—
(4,4)	$< 2.1 (3\sigma)$	$< 0.1$	—	—	$< 0.4$	—	—